

1 **Influence of enhanced Asian NO_x emissions on ozone in the Upper Troposphere and** 2 **Lower Stratosphere (UTLS) in chemistry climate model simulations**

3 Chaitri Roy¹, Suvarna Fadnavis^{1*}, Rolf Müller², Ayantika D. C.¹, Felix Ploeger², Alexandru Rap³

4 ¹Indian Institute of Tropical Meteorology, Pune, India

5 ²Forschungszentrum Jülich GmbH, IEK7, Jülich, Germany

6 ³School of Earth and Environment, University of Leeds, Leeds, United Kingdom

7 *Email of corresponding author: suvarna@tropmet.res.in

8 **Abstract:**

9 The Asian summer monsoon (ASM) anticyclone is the most pronounced circulation pattern in the
10 Upper Troposphere and Lower Stratosphere (UTLS) during Northern Hemisphere summer. Asian
11 summer monsoon convection plays an important role in efficient vertical transport from the surface to
12 the upper-level anticyclone. In this paper we investigate the potential impact of enhanced
13 anthropogenic nitrogen oxide (NO_x) emissions on the distribution of ozone in the UTLS using the
14 fully-coupled aerosol chemistry climate model, ECHAM5-HAMMOZ. Ozone in the UTLS is
15 influenced both by the convective uplift of ozone precursors and by the uplift of enhanced NO_x induced
16 tropospheric ozone anomalies. We performed anthropogenic NO_x emission sensitivity experiments over
17 India and China. In these simulations, covering the years 2000-2010 anthropogenic NO_x emissions
18 have been increased by 38% over India and by 73% over China with respect to the emission base year
19 2000. These emission increases are comparable to the observed linear trends of 3.8 % per year over
20 India and 7.3% per year over China during the period 2000 to 2010. Enhanced NO_x emissions over
21 India by 38 % and China by 73 % increase the ozone radiative forcing in the ASM Anticyclone (15°-
22 40°N, 60°-120°E) by 16.3 mW m⁻² and 78.5 mW m⁻² respectively. These elevated NO_x emissions
23 produce significant warming over the Tibetan Plateau and increase precipitation over India due to a
24

25 strengthening of the monsoon Hadley circulation. However increase in NO_x emissions over India by
26 73% (similar to the observed increase over China), results in large ozone production over the Indo
27 Gangetic plain and Tibetan Plateau. The higher ozone concentrations, in turn, induce a reversed
28 monsoon Hadley circulation and negative precipitation anomalies over India. The associated
29 subsidence suppresses vertical transport of NO_x and ozone into the ASM anticyclone.

30 Key words: Asian summer monsoon, Tropospheric ozone, Tropospheric NO_x , NO_x transport, Upper
31 troposphere and lower stratosphere, Ozone radiative forcing.

32

33 **1. Introduction**

34 Rapid economic development and urbanization in Asia has resulted in an unprecedented growth in
35 anthropogenic emissions of nitrogen oxides (NO_x), carbon monoxide (CO), carbon dioxide (CO_2),
36 methane (CH_4). Many of these species affect concentrations of tropospheric ozone, which is both an
37 important polluting agent and a greenhouse gas (Wild and Akimoto, 2001; Chatani et al 2014; Revell et
38 al., 2015). Ground based and satellite observations show a large amount of these ozone precursors
39 concentrated over India and China (Sinha et al., 2014; Richter et al., 2005; Jacob et al., 1999; Zhao et
40 al., 2013; Gu et al., 2014). Studies show that tropospheric ozone production over Asia is controlled by
41 the abundance of NO_x and VOCs (Sillman, 1995, Lei et al., 2004, Zhang et al., 2004 and Tie et al.,
42 2007), with large regions such as India and China being NO_x limited regions. Therefore, increased NO_x
43 in these regions leads to an increase in ozone concentrations (Yamaji et al., 2006; Sinha et al., 2014;
44 Fadnavis et al., 2014). Recently, positive trends in Asian tropospheric column NO_2 have been reported,
45 i.e. 3.8 \% yr^{-1} over India, using SCanning Imaging Absorption SpectroMeter for Atmospheric
46 CHartography (SCIAMACHY) observations for the period 2003-2011 (Ghude et al., 2013), and 7.3%
47 yr^{-1} over China using Ozone Monitoring Instrument (OMI) observations for the period 2002-2011
48 (Schneider and van der A., 2012). Lightning contributes to the production of NO_x in the middle and

49 upper troposphere (Barret et al, 2016). Over the Asian region, lightning contributes ~40% to NO_x and
50 20% to ozone production in the middle and upper troposphere during the monsoon season (Tie et al.
51 2001; Fadnavis et al. 2015). The upper tropospheric ozone concentration is determined by in-situ
52 production from both lightning and ozone precursors which are transported from the boundary layer
53 (Sóvde et al., 2011; Barret et al, 2016).

54 Tropospheric ozone has a warming effect on climate, its estimated radiative forcing due to
55 increased concentrations since pre-industrial times being 0.4 W m⁻², with a 5 to 95% confidence range
56 of (0.2 to 0.6 W m⁻²) (Stevenson et al., 2013; Myhre et al., 2013). Previous studies highlighted the
57 importance of the tropical tropopause region for ozone radiative forcing (Lacis et al, 1990; Riese et al.,
58 2012; Rap et al., 2015) and showed that ozone perturbations exert a large influence on the thermal
59 structure of the atmosphere (e.g., Thuburn and Craig, 2002; Foster and Shine 1997). A recent study
60 based on Atmospheric Chemistry and Climate Model Intercomparison Project (ACCMIP) models
61 reported that NO_x and CH₄ are the greatest contributors in determining tropospheric ozone radiative
62 forcing (Stevenson et al., 2013).

63 Asian Summer Monsoon (ASM) convection efficiently transports Asian pollutants from the
64 boundary layer into the Upper Troposphere and Lower Stratosphere (UTLS) (Randel and Park, 2006;
65 Randel et al. 2010; Fadnavis et al., 2013, 2015). Studies pertaining to modeling and trajectory analysis
66 confirm this finding (Li et al., 2005; Park et al., 2007; Randel et al., 2010; Chen et al., 2012; Vogel et
67 al., 2015, 2016). Satellite observations show the confinement of a number of chemical constituents like
68 water vapor (H₂O), CO, CH₄, ethane, hydrogen cyanide (HCN), PAN and aerosols, within the ASM
69 anticyclone (Park et al., 2004, 2007, 2008; Li et al., 2005; Randel and Park, 2006; Xiong et al., 2009;
70 Randel et al. 2010; Lawrence et al., 2011; Abad et al., 2011; Fadnavis et al., 2013;2014;2015; Barret et
71 al., 2016) which has potential implications on stratospheric chemistry and dynamics. Thus the rise in
72 anthropogenic emissions over the ASM region alters the chemical composition of the UTLS (Lawrence

73 et al., 2011; Fadnavis et al, 2014, 2015) during the monsoon season. Another prominent feature of the
74 satellite observations is an ozone minimum in the ASM anticyclone (near 100 hPa) (Gettelman et al.,
75 2004; Konopka et al., 2010; Braesicke et al., 2011). This ozone minimum is linked to upward transport
76 of ozone poor air masses (Gettelman et al., 2004; Park et al., 2007; Kunze et al., 2010). Observations
77 show that convectively lifted air masses arriving in the anticyclone are ozone poor but rich in ozone
78 precursors. Balloon sonde observations show that ozone variations near the anticyclone are strongly
79 correlated with temperature near the tropopause (Tobo et al., 2008). Thus the linkage of low ozone and
80 high concentrations of ozone precursors with the temperature variation in the anticyclone is an open
81 question.

82 In this study we ask the question ‘how do increasing Asian NO_x emissions and the associated
83 ozone production affect ozone radiative forcing and monsoon circulation?’. We perform sensitivity
84 experiments of increased anthropogenic NO_x emissions using the state-of-the-art ECHAM5-HAMMOZ
85 (European Centre General Circulation Model version5) chemistry climate model (Roeckner et al.,
86 2003; Horowitz et al., 2003; Stier et al., 2005). We estimate the ozone radiative forcing for the different
87 anthropogenic NO_x emission scenarios, together with associated changes in temperature and the
88 monsoon circulation. The paper is organized as follows: in Section 2 the data and model set up are
89 described; the results are summarized in Section 3 and discussed in Section 4, followed by conclusions
90 given in Section 5.

91

92 **2. Data description and Model setup**

93 **2.1 Satellite measurements**

94 Earth Observing System (EOS) microwave limb sounder (MLS) is one of the four instruments
95 on the NASA’s EOS Aura satellite flying in the polar sun-synchronous orbit. It measures the thermal
96 emissions at millimeter and sub millimeter wavelengths (Waters et al., 2006). It performs 240 limb

97 scans per orbit with a footprint of ~ 6 km across-track and ~ 200 km along-track, providing ~ 3500
98 profiles per day. MLS also measures vertical profiles of temperature, ozone, CO, H₂O, and many other
99 constituents in the mesosphere, stratosphere and upper troposphere (Waters et al., 2006). In the UTLS,
100 MLS has a vertical resolution of about 3 km. MLS vertical profiles of ozone show good agreements
101 with the Stratospheric Aerosol and Gas Experiment II (SAGE-II), Halogen Occultation Experiment
102 (HALOE), Atmospheric Chemistry Experiment (ACE) and ozonesonde measurements (Froidevaux et
103 al., 2006). The MLS ozone profiles are considered to be useful in the range of 215 – 0.46 hPa (Livesey
104 et al., 2005). In this study we analyze the MLS level 2 (version 4) ozone mixing ratios data for the
105 period 2004 – 2013. The data has been gridded horizontally, within latitude bins of equal area (with the
106 equatorial bin of 150km width) and longitude bins of about 8.5 degrees. This data can be accessed from
107 <http://mls.jpl.nasa.gov/>. For comparison, simulated ozone is convolved with the MLS averaging kernel
108 (Livesey et al. 2011).

109

110 **2.2 Model simulation and experimental setup**

111 We employ the aerosol-chemistry-climate model ECHAM5-HAMMOZ which comprises the
112 general circulation model ECHAM5 (Roeckner et al., 2003), the tropospheric chemistry module,
113 MOZART2 (Horowitz et al 2003) and the aerosol module, Hamburg aerosol model (HAM) (Stier et al.,
114 2005). It includes NO_x, VOC and aerosol chemistry. The gas phase chemistry is based on the chemical
115 scheme provided by the MOZART-2 model (Horowitz et al., 2003) which includes detailed chemistry
116 of the O_x-NO_x hydrocarbon system with 63 tracers and 168 reactions. The O(¹D) quenching reaction
117 rates used are taken from Sander et al., (2003) and isoprene nitrates chemistry taken from Fiore et al.,
118 (2005). The dry deposition in ECHAM5-HAMMOZ follows the scheme given by Ganzeveld and
119 Lelieveld (1995). Soluble trace gases like HNO₃ and SO₂ are also subject to wet deposition. In-cloud
120 and below-cloud scavenging follows the scheme given by Stier et al. (2005). Interactive calculation of

121 cloud droplet number concentration is according to Lohmann et al (1999) and ice crystal number
122 concentrations are according to Kärcher and Lohmann (2002). The convection scheme is based on the
123 mass flux scheme developed by Tiedke (1989). Lightning NO_x emissions are parameterized following
124 Grewe et al. (2001).

125 The model is run at a T42 spectral resolution corresponding to about 2.8°×2.8° in the horizontal
126 dimension and 31 vertical hybrid $\sigma - p$ levels from the surface to 10 hPa. In our model simulations,
127 emissions from anthropogenic sources and biomass burning are from the year 2000 RETRO project
128 data set (available at <http://eccad.sedoo.fr/>) (Schultz et al., 2004; 2005; 2007; 2008). Emissions of SO₂,
129 BC and OC are based on the AEROCOM-II emission inventory, also for the year 2000 (Dentener et al.,
130 2006). The distribution of NO_x emission mass flux ($\text{kg m}^{-2} \text{s}^{-1}$) averaged for the Asian summer
131 monsoon season (June–September) is shown in Supplementary Fig. S1. It shows high values over the
132 Indo Gangetic Plains and East China. Other details of model parameterizations, emissions and
133 evaluation are described by Fadnavis et al. (2013; 2014; 2015) and Pozzoli et al. (2008a, b; 2011). Each
134 of our model experiments consists of continuous simulations for eleven years from 2000 to 2010. The
135 base year for emissions is taken as 2000 and emissions were repeated every year throughout the
136 simulation period. Meteorology varied due to varying monthly mean sea surface temperature (SST) and
137 sea ice concentration (SIC). The AMIP2 SSTs and SIC varying for the period 2000 – 2010 were
138 specified as a lower boundary condition.

139 In order to understand the impact of enhanced anthropogenic NO_x emissions on the distribution
140 of ozone in the UTLS, sensitivity simulations were performed for the period 2000 – 2010. The
141 experimental set up is the same as described by Fadnavis et al. (2015). The four simulations analyzed
142 in this study are: (1) a reference experiment (CTRL) and three sensitivity experiments (referred to as
143 experiments 2 - 4), where the anthropogenic NO_x emissions over India and China are scaled in
144 accordance with the observed trends. In experiment (2), anthropogenic NO_x emissions are increased

145 over India by 38% (Ind38), in experiment (3) increases over China by 73% (Chin73) are prescribed. In
146 order to analyze the effects of similar NO_x percentage increases over India and China, NO_x emissions
147 are increased over India by 73% (Ind73) in experiment (4). The emission perturbations were obtained
148 from observed NO₂ trends of 3.8% per year over India (Ghude et al., 2013) and 7.3% per year over
149 China (Schneider and van der A., 2012). Hiboll et al. (2013) also reported similar increasing NO_x
150 values over megacities in India and China. All four simulations use the same VOC and CO emissions
151 and they all include NO_x production due to lightning (lightning-on) and soil emissions. There may be
152 indirect impact of lightning NO_x emission. Since it is same in CTRL and sensitivity simulations its
153 impact may be negligible.

154 In addition, a lightning-off simulation was performed for the same period and boundary
155 conditions as experiments 1-4 (this simulation is the same as the one described in Fadnavis et al.
156 (2015)). The impact of lightning on NO_x production is estimated by comparing the CTRL (lightning-
157 on) with lightning-off simulations.

158 The accuracy of the simulation of the monsoon circulation probably depends on model
159 resolution and an increased vertical resolution may improve the model performance (Druryan et al.,
160 2008; Abhik et al., 2014). However, the model resolution of T42L31 is capable of reasonably
161 simulating the general regional spatial pattern of precipitation and low-level circulation (Rajeevan et
162 al., 2005) (see Supplementary Fig. S2, showing simulated seasonal mean precipitation and circulation
163 at 850 hPa in the CTRL simulation).

164 The heating rates and radiative forcings associated with the ozone changes in our three
165 sensitivity simulations are calculated using the Edwards and Slingo (1996) radiative transfer model and
166 the fixed dynamical heating approximation for stratospheric temperature adjustment. Similarly to
167 previous studies (Riese et al., 2012; Bekki et al., 2013; Rap et al., 2015), we used the off-line version of
168 the model, with six shortwave and nine longwave bands, and a delta-Eddington 2-stream scattering

169 solver at all wavelengths.

170

171 **3. Results**

172 **3.1 Comparison with MLS satellite measurements in the UTLS**

173 The spatial distributions of ozone mixing ratios from MLS observations at 100 hPa and from
174 the CTRL ECHAM5-HAMMOZ simulation at 90 hPa (the nearest model level) after smoothing with
175 the averaging kernel of MLS are illustrated in Fig. 1a and Fig. 1b, respectively. For comparison we
176 have interpolated the model data to the MLS pressure grid, then applied the MLS averaging kernel and
177 finally interpolated back to the model pressure grid. The climatological horizontal winds plotted in the
178 figure clearly show the anticyclonic upper level monsoon circulation. Recent attempts to characterize
179 the extent of the anticyclone are based either on potential vorticity on isentropic surfaces or
180 geopotential height on pressure surfaces. Here we apply both characterizations of the anticyclone and
181 show the PV contour related to the maximum PV gradient on 380K (calculated from ERA-Interim
182 reanalysis following Ploeger et al., 2015), and the 270m geopotential height anomaly as proposed by
183 Barret et al. (2016). The close agreement of both methods shows that from a climatological point of
184 view the two criteria yield a very similar picture of the anticyclonic circulation and the related trace gas
185 confinement. Locally and at particular dates, however, differences may be larger with potential
186 vorticity correlating better with confined trace gas anomalies than geopotential height (e.g., Garny and
187 Randel, 2013; Ploeger et al., 2015). The spatial pattern of low ozone concentrations in the monsoon
188 anticyclone is well simulated in the model. It is in good agreement with MLS (90-140 ppbv), MIPAS
189 (80-120 ppbv) and SAGE II (<150ppbv) measurements (Kunze et al., 2010; Randel et al., 2001; Randel
190 and Park 2006; Park et al., 2007).

191 Vertical profiles of ozonesonde measurements (averaged for the monsoon season during 2001-
192 2009) at Indian stations, Delhi (28.61°N, 77.23°E), Pune (18.52°N, 73.85°E) and Thiruvananthapuram

193 (8.48°N, 76.95E) are compared with MLS measurements and ECHAM5-HAMMOZ simulated ozone
194 mixing ratios in Figs. 1(c)-(e). ECHAM5-HAMMOZ simulations show good agreement with MLS data
195 between 200 hPa and 50 hPa at all three stations. Comparison of ozonesonde observations with the
196 ECHAM5-HAMMOZ simulation shows reasonably good agreement at Pune, compared to Delhi and
197 Thiruvananthapuram where there are some discrepancies. The simulated ozone mixing ratios are lower
198 than ozonesonde measurements by 10-40 ppb between 500 – 90 hPa at Pune and by ~70-90 ppb in the
199 upper troposphere (500-150 hPa) at Delhi. At Thiruvananthapuram, while at altitudes below 375 hPa,
200 simulated ozone mixing ratios show good agreement with ozonesonde data, at the altitudes above 375
201 hPa, simulated values are lower than observations by ~20-70 ppb. The differences between model and
202 ozonesonde data may be due to different grid sizes: the ECHAM5-HAMMOZ model grid size is ~280
203 km, while balloon observations are within ~30-180 km spatial range (balloon typically drifts ~30–180
204 km horizontally). In addition, previous work comparing these model simulations with various aircraft
205 observations during the monsoon season, found a reasonable agreement for PAN, NO_x, HNO₃ and O₃
206 mixing ratios (Fadnavis et al., 2015).

207

208 **3.2 Transport of enhanced NO_x emissions into the UTLS**

209 Recent satellite observations and model simulations demonstrated the impact of convective
210 transport of boundary layer pollution into the ASM anticyclone during the Asian summer monsoon
211 season (Gettelman et al., 2004; Randel et al., 2010; Fadnavis et al., 2013, 2014, 2015). These pollutants
212 are further transported across the tropopause as evident in satellite observations of, e.g. water vapour
213 (Bian, 2012), hydrogen cyanide (HCN) (Randel, 2010), CO (Schoeberl et al., 2006), Peroxyacetyl
214 nitrate (PAN) (Fadnavis et al., 2014; 2015), aerosols (Vernier et al., 2015, Fadnavis et al., 2013). To
215 understand the influence of monsoon convection on the vertical distribution of NO_x we show zonal and
216 meridional cross sections over India and China. Vertical distributions of NO_x averaged for the monsoon

217 season over Indian latitudes (8°N - 35°N), and Chinese latitudes (20°N - 45°N) as obtained from CTRL
218 simulations are shown in the Supplementary Figs. S3(a) and S3(b) respectively. These figures show
219 elevated levels of NO_x extending from the surface to the upper troposphere over India and China. The
220 wind vectors along with the distribution of cloud droplet number concentration (CDNC) and ice crystal
221 number concentration (ICNC), (Supplementary Figs. S4(a), S4(b) and S4(c)) indicate strong convective
222 transport from the Bay of Bengal (BOB), South China Sea and southern slopes of Himalayas which
223 might lift the boundary layer NO_x to the upper troposphere.

224 During the monsoon season, the NO_x distribution in the UTLS is also influenced by lightning,
225 in addition to transport from anthropogenic sources. Lightning activity during this season was found to
226 be more pronounced in Asia, compared to the other monsoon regions such as North America, South
227 America and Africa (Ranalkar and Chaudhari, 2009; Penki and Kamra, 2013). In our simulations, we
228 find that lightning produces 40-70% of NO_x over north India and Bay of Bengal and 40-60% over the
229 Tibetan Plateau and West China region (Supplementary Fig. S5).

230 Fig. 2 shows the vertical distribution of anthropogenic NO_x anomalies obtained from the Ind38,
231 Ind73, Chin73 simulations, compared with the CTRL simulation. Ind38 simulation shows that the
232 convective winds over the Bay of Bengal (80 - 90°E) (Fig. 2(a)) and at the southern flank of the
233 Himalayas (Fig. 2(d)) lift up the enhanced Indian NO_x emissions to the upper troposphere (UT).
234 Similarly the Chin73 simulation shows that the convective winds over the South China Sea (100 -
235 120°E) (Fig. 2(c)) and over the Himalayas (Fig. 2(f)) lift up the enhanced Chinese NO_x emissions to the
236 UT. While most transport is mainly into the UT, parts of it also occur into the lower stratosphere, with
237 cross tropopause transport being particularly evident in the Chin73 simulation (Figs. 2(c) and 2(f)).
238 Randel and Park (2006) and Randel et al. (2010) also reported that pollution transported by Asian
239 monsoon convection enters the stratosphere. Our results are also in good agreement with previous
240 studies indicating significant vertical transport due to strong monsoon convection from the southern

241 slopes of Himalayas (Fu et al., 2006, Fadnavis et al., 2013; 2014) and the South China Sea (Park et al
242 2009; Chen et al., 2012). In the upper troposphere, NO_x is transported over Iran and Saudi Arabia along
243 the descending branch of the large scale monsoon circulation (Rodwell and Hoskins, 1995). However,
244 the cross tropopause transport is not present in the Ind73 simulation, where it is inhibited by the wind
245 anomalies that show a descending branch over central India ($\sim 20^\circ\text{N}$, 75°E) (Figs. 2(b) and 2(e)). These
246 descending wind anomalies may also be related to the associated ozone radiative forcing and
247 temperature changes, as discussed in Section 4.

248

249 **3.3 Impact of enhanced anthropogenic NO_x on the tropospheric ozone distribution**

250 We calculate the change in ozone production over India and China due to enhanced NO_x
251 emissions in the Ind38, Ind73 and Chin73 simulations with respect to the CTRL simulation. Figure 3,
252 showing longitude-pressure cross sections of net ozone production (ppt/day) changes, indicates that the
253 majority of this additional ozone production occurs in the lower troposphere. At altitudes below 300
254 hPa, the ozone production and loss vary between -15 ppt day^{-1} and 15 ppt day^{-1} . In the upper
255 troposphere (300-150 hPa), the estimated amount of additional net ozone production in Ind38 and
256 Ind73 simulation is $3\text{-}7 \text{ ppt day}^{-1}$, while in the Chin73 simulation it is $\sim 3\text{-}13 \text{ ppt day}^{-1}$. We also simulate
257 ozone loss near the tropopause in the Ind73 simulation (Fig. 3(b)). We note that these ozone anomalies
258 are not driven by lightning NO_x , as this is included in all simulations. It is interesting to understand
259 ozone production over the highly populated Indo Gangetic Plain and Tibetan Plateau region (these
260 regions are marked in Fig. S4). A longitude pressure cross section over this region show that ozone
261 production over the Indo Gangetic Plain and Tibetan Plateau in Ind73 is ($20\text{-}25 \text{ ppt day}^{-1}$) is much larger
262 than Ind38 ($6\text{-}20 \text{ ppt day}^{-1}$) in the lower troposphere (Supplementary Fig. S6).

263 Figure 4 shows the vertical distribution of ozone anomalies induced by enhanced anthropogenic
264 NO_x emissions in the three perturbation experiments compared to the CTRL simulation, averaged over

265 India and China. Although the air mass in the monsoon anticyclone is relatively poor in ozone
266 (Fig.1(b)), the elevated amounts of ozone anomalies in response to enhanced anthropogenic NO_x
267 emissions are clearly seen in Fig. 4. This may be partially due to convective transport of enhanced-
268 NO_x -emission induced ozone anomalies produced in the lower troposphere, and partially due to
269 chemical ozone production from convectively transported boundary layer ozone precursors. Ozone
270 anomalies are enhanced near 300-200 hPa over west Asia (40-60°E) (Figs. 4a-c), possibly due to the
271 vertical convective transport of ozone anomalies and precursors and also from subsequent horizontal
272 transport in the monsoon anticyclone (Barret et al., 2016).

273 Latitude-pressure cross sections of enhanced NO_x emission induced ozone anomalies plotted in
274 Figs. 4(d) and 4(f) illustrate how convection over the Bay of Bengal, the southern slopes of the
275 Himalayas and the South China Sea lifts the enhanced ozone anomalies from India and China into the
276 upper troposphere. These ozone anomalies are also transported further across the tropopause and into
277 the lower stratosphere, where ozone production is also driven by photolysis and NO_x anomalies.

278 In the Ind73 simulation, similarly to the NO_x anomaly distribution (Figs. 2(b) and 2(e)), the
279 descending branch of circulation over central India also suppresses the vertical transport of ozone
280 anomalies across the tropopause (Figs. 4(b) and 4(e)). This subsidence may be related to ozone heating
281 rate changes, as there is significant increase in ozone production over the Indo Gangetic plain and
282 Tibetan Plateau in the lower troposphere due to enhanced anthropogenic NO_x emissions (Section 4).

283

284 **3.4 Distribution of NO_x and ozone in the anticyclone**

285 The distributions of NO_x and ozone anomalies in the monsoon anticyclone region in the Ind38,
286 Ind73 and Chin73 simulations with respect to the CTRL simulation are shown in Figs. 5(a)-(f). A
287 maximum in the NO_x anomalies in the ASM anticyclone (60°E to 120°E) is seen in all the simulations.
288 NO_x anomalies are high at the eastern part of the monsoon anticyclone since convective injection into

289 the anticyclone occurs mainly in that region (Fadnavis et al., 2013). Increase in NO_x anomalies in the
290 Ind38 simulation is higher (Fig. 5(a)) than that in the Ind73 simulation (Figs. 5(b)), mainly due to
291 descending motion over central India in the Ind73 simulation, as seen in the previous sections. In
292 contrast to NO_x anomalies, ozone anomalies in Ind38 are lower than Ind73, especially in the north-
293 eastern part of anticyclone. Satellite observations also show high ozone precursors and low ozone
294 amounts in the anticyclone (Park et al., 2007; Barret et al., 2016). Similarly, the Chin73 simulation
295 shows higher values of NO_x anomalies (>18%) and strong negative ozone anomalies (~-8%) in the
296 north eastern region of the monsoon anticyclone (Figs. 5(c) and 5(f)). Figure 5 also shows that the
297 tropical easterly jet transports NO_x and ozone (from India and China) to Saudi Arabia, Iran and Iraq.

298

299 **4. Discussion**

300 To estimate the radiative impact of the simulated ozone changes, we use the offline version of
301 the Edwards and Slingo (1996) radiative transfer model. Figure 6 shows the radiative forcing caused by
302 the ozone changes in each of the three sensitivity simulations compared to the CTRL simulation. The
303 overall increase in tropospheric ozone (see Figure 4) has a warming effect on climate, with the regional
304 average radiative forcing in the monsoon anticyclone (15°N-40°N, 60-120°E) estimated at 16.3 mW m^{-2} ,
305 69.9 mW m^{-2} , and 78.5 mW m^{-2} in the Ind38, Ind73, and Chin73 simulations, respectively.

306 We also investigate the impact on the atmospheric heating rates caused by the ozone changes.
307 Figure 7 shows the zonal mean heating rate anomalies for the Ind38, Ind73 and Chin73 simulations,
308 compared to the CTRL simulation. These three simulations show positive and negative heating rates
309 anomalies between 400-200 hPa. However, in the upper troposphere and lower stratosphere (200-50
310 hPa) ozone heating rates are negative over Indo Gangetic plain (20-30°N) and Tibetan Plateau (30-
311 40°N) region. In Ind73 simulation, ozone heating rate anomalies are positive in the lower troposphere
312 over the Indo Gangetic plain (1000-750 hPa) and Tibetan plateau (600-400 hPa). This may be due to

313 large amount of ozone production in the lower troposphere over these regions (Fig. S6). This heating
314 may produce changes in the circulation leading to ascending motion over the Tibetan Plateau and a
315 descending branch over central India ($\sim 20^\circ\text{N}$), i.e. a reversal of monsoon Hadley circulation (Fig. 9(b)).

316 Figures 8 shows latitude pressure cross-section of temperature anomalies (K) obtained from
317 Ind38, Ind73 and Chin73 simulations. Ind38 and Chin73 simulations show anomalous warming in the
318 upper troposphere over the Tibetan Plateau while it is subdued in the Ind73 simulation. Upper
319 tropospheric warming over the Tibetan plateau is one of the key factors responsible for the ASM
320 circulation (Flohn 1957; Yanai et al., 1992; Meehl, 1994; Li and Yanai, 1996; Wu and Zhang, 1998).
321 Flohn (1957, 1960) suggested that upper tropospheric warming over the Tibetan plateau leads to
322 increased Indian summer monsoon rainfall by enhancing the cross-equatorial circulation that brings
323 rainfall to India (Rajagopalan and Molnar, 2013, Vinoj et al., 2014). Goswami et al., (1999) also
324 reported that there is a strong correlation between Hadley circulation and monsoon precipitation.

325 Figures 9(a)-(c) depict the change in monsoon Hadley cell circulation (averaged over 70°E -
326 100°E) obtained from the difference in the Ind38, Ind73 and Chin73 and CTRL simulations. The Ind38
327 and Chin 73 simulations show a strengthening of the Hadley circulation; a strong ascending branch of
328 the Hadley cell around 10° - 20°N (Fig. 9(a)), whereas the tilted descending branch of Hadley cell is seen
329 over 20°N in the Ind73 simulation (Fig. 9(b)). In Ind73 simulation ozone heating rates are positive and
330 negative in the vertical direction near $\sim 20^\circ\text{N}$ (Fig 7 (b)) which might have attributed tilted descending
331 branch of Hadley cell. Consequently, precipitation anomalies over the Indian region (70° - 90°E ; 8° - 35°
332 N) are positive (0.3 to 0.9 mm day^{-1}) in the Ind38 and Chin73 simulations (Figs. 9(d) and 9(f)), whereas
333 they are negative in the Ind73 simulation (-0.3 to -0.6 mm day^{-1}) (Fig. 9(e)). In the upper troposphere
334 (250 hPa - 100 hPa), Ind73 simulation shows subsidence while Chin73 simulation shows ascending
335 motion at these levels over the Indian region. Upper tropospheric subsidence in Ind73 simulation might
336 have contributed to the weak positive and negative precipitation anomalies over the North Indian

337 region (Fig. 9(e)). The Chin73 simulation shows subsidence near 22°N below 200 hPa and ascending
338 motion above it. The Chin73 simulation shows ascending motion near 12°N rising up to 110 hPa, which
339 leads to positive precipitation anomalies over the Indian peninsula.

340 Thus, enhanced Indian (Ind38) and Chinese (Chin73) NO_x emissions increase warming over the
341 Tibetan plateau and enhance precipitation over India via a strengthening of the monsoon Hadley
342 circulation. Remarkably, a further increase of NO_x emissions over India (Ind73) leads to high amounts
343 of ozone in the lower troposphere over the Indo Gangetic plain and Tibetan Plateau. The related ozone
344 heating induces a reversal of the monsoon Hadley circulation, thereby resulting in negative
345 precipitation anomalies.

346 **5. Conclusions**

347 In this paper we investigate the potential impacts of enhanced anthropogenic NO_x emissions on
348 ozone production and distribution during the monsoon season using the state-of-the-art ECHAM5-
349 HAMMOZ model simulations. We performed sensitivity experiments for anthropogenic NO_x
350 enhancements of 38% over India (Ind38 simulation) and 73% over China (Chin73 simulation) in
351 accordance with recently observed trends of 3.8% per year over India and 7.3% per year over China
352 (Ghude et al., 2013; Schneider and van der A., 2012). In another experiment, anthropogenic NO_x
353 emissions over India are increased by 73%, equal to Chinese emissions (Ind73 simulation).

354 These simulations show that an increase in anthropogenic NO_x emissions (over India and
355 China) increases ozone production in the lower and mid-troposphere. The monsoon convection at the
356 southern flank of the Himalayas (80-90°E) and over the Bay of Bengal lifts up the NO_x and ozone
357 anomalies from India across the tropopause into the lower stratosphere (Fig. 2(a)-(c), Fig. 4(a)-(b) and
358 Fig. S4). Cross tropopause transport also occurs over China due to convection over the South China
359 Sea.

360 Increase in NO_x emissions in the Ind38, Ind73 and Chin73 simulations leads to increase in
361 ozone radiative forcings, in the anticyclone (15°N - 40°N , 60°E - 120°E) of 16.25 mWm^{-2} , 69.88 mW m^{-2} ,
362 and 78.51 mW m^{-2} in the Ind38, Ind73, and Chin73 simulations, respectively. Enhanced ozone
363 production (Ind38 and Chin73 simulations) increases ozone heating rates which cause anomalous
364 warming over the Tibetan plateau. Further increase in NO_x emissions over the India region (Ind73
365 simulation) produces anomalous heating in the lower troposphere over the Indo Gangetic Plain and
366 Tibetan Plateau. This warming elicits the reversal of the monsoon Hadley cell circulation. The
367 descending branch of the monsoon Hadley circulation over the central India impedes vertical transport
368 of ozone and NO_x anomalies.

369 In the Ind38 and Chin73 simulations, anomalous warming over the Tibetan plateau results in a
370 strengthening of the monsoon Hadley circulation over India and elicits positive precipitation (0.3 to 0.9
371 mm day^{-1}) anomalies over India. However, in Ind73 simulations the reversal of the Hadley circulation
372 and the concurrent subdued warming in the upper troposphere over the Tibetan plateau results in
373 negative precipitation anomalies (-0.3 to -0.6 mm day^{-1}) over India.

374

375 *Acknowledgement:* Dr. S. Fadnavis and C. Roy acknowledges with gratitude Dr. Krishnan, Director of
376 IITM, for his encouragement during the course of this study. We also thank two anonymous reviewers
377 for their valuable suggestions for improvement of this manuscript. The authors acknowledge the High
378 Power Computing Centre (HPC) in IITM, Pune, India, for providing computer resources. Part of the
379 research leading to these results has received funding from the European Community's Seventh
380 Framework Programme (FP7/2007-2013) in the frame of the StratoClim project under grant agreement
381 number 603557. Felix Ploeger was supported by the Helmholtz Young Investigators Group grant A-
382 SPECi (VH-NG-1128).

383

384 **References:**

- 385 Abad G. G., Allen N. D. C., Bernath P. F., Boone C. D., McLeod S. D., Manney G. L., Toon G. C.,
386 Carouge C., Wang Y., Wu S., Barkley M. P., Palmer P. I., Xiao Y., and Fu T. M.: Ethane, ethyne
387 and carbon monoxide concentrations in the upper troposphere and lower stratosphere from ACE
388 and GEOS-Chem: a comparison study, *Atmos. Chem. Phys.*, 11, 9927–9941, 2011.
389 doi:10.5194/acp-11-9927-2011, 2011.
- 390 Abhik S., Mukhopadhyay P., Goswami B. N., Evaluation of mean and intraseasonal variability of
391 Indian summer monsoon simulation in ECHAM5: identification of possible source of bias,
392 *Climate Dynamics*, 43 (1), pp. 389–406, 2014.
- 393 Barret, B., Sauvage, B., Bennouna, Y., and Le Flochmoen, E.: Upper-tropospheric CO and O₃ budget
394 during the Asian summer monsoon, *Atmos. Chem. Phys.*, 16, 9129-9147, doi:10.5194/acp-16-
395 9129-2016, 2016.
- 396 Bekki, S., Rap, A., Poulain, V., Dhomse, S., Marchand, M., Lefevre, F., Forster, P. M., Szopa, S. and
397 Chipperfield, M. P.: Climate impact of stratospheric ozone recovery, *Geophys. Res. Lett.*,
398 40(11),2796-2800,doi:10.1002/grl.50358,2013.
- 399 Bian, J., Pan, L. L., Paulik, L., Vömel, H., Chen, H., and Lu, D.: In situ water vapor and ozone
400 measurements in Lhasa and Kunming during the Asian summer monsoon, *Geophys. Res. Lett.*,
401 39, L19808, doi:10.1029/2012GL052996, 2012.
- 402 Braesicke, P., Smith, O. J., Telford, P., & Pyle, J. A.: Ozone concentration changes in the Asian
403 summer monsoon anticyclone and lower stratospheric water vapour: An idealised model study.
404 *Geophysical Research Letters*, 38(3), doi: 10.1029/2010GL046228, 2011.
- 405 Chatani, S., Amann, M., Goel, A., Hao, J., Klimont, Z., Kumar, A., Mishra, A., Sharma, S., Wang, S.
406 X., Wang, Y. X., and Zhao, B.: Photochemical roles of rapid economic growth and potential
407 abatement strategies on tropospheric ozone over South and East Asia in 2030, *Atmos. Chem.*
408 *Phys.*, 14, 9259-9277, doi:10.5194/acp-14-9259-2014, 2014.
- 409 Chen, B., Xu, X., D, Yang, S., and Zhao, T. L.: Climatological perspectives of air transport from
410 atmospheric boundary layer to tropopause layer over Asian monsoon regions during boreal
411 summer inferred from Lagrangian approach, *Atmos. Chem. Phys.*, 12, 5827–5839,
412 doi:10.5194/acp-12-5827-2012. 2012.
- 413 Dentener F., Kinne S., Bond T., Boucher O., Cofala J., Generoso S., Ginoux P., Gong S., Hoelzemann
414 J. J., Ito A., Marelli L., Penner J. E., Putaud J.-P., Textor C., Schulz M., Werf G. R. van der, and
415 Wilson J.: Emissions of primary aerosol and precursor gases in the years 2000 and 1750
416 prescribed data-sets for AeroCom, *Atmos. Chem. Phys.*, 6, 4321-4344, doi:10.5194/acp-6-
417 4321-2006, 2006.
- 418 Druyan L. M., Fulakeza M. and Lonergan P.: The impact of vertical resolution on regional model
419 simulation of the west African summer monsoon, *Int. J. Climatol.* 28: 1293–1314, DOI:
420 10.1002/joc.1636, 2008.
- 421 Edwards, J. M., and Slingo, A.: Studies with a flexible new radiation code .1. Choosing a
422 configuration for a large-scale model, *Quart. Jour. Roy. Met. Soc.*, 122(531), 689-719,
423 doi:10.1002/qj.49712253107,1996.
- 424 Fadnavis, S., Semeniuk, K., Pozzoli, L., Schultz, M. G., Ghude, S. D., Das, S., and Kakatkar, R.:
425 Transport of aerosols into the UTLS and their impact on the Asian monsoon region as seen in a
426 global model simulation, *Atmos. Chem. Phys.*, 13, 8771–8786, doi:10.5194/acp-13-8771-2013,
427 2013.
- 428 Fadnavis, S., Semeniuk, K., Schultz, M. G., Kiefer, M., Mahajan, A., Pozzoli, L., and Sonbawane, S.:
429 Transport pathways of peroxyacetyl nitrate in the upper troposphere and lower stratosphere
430 from different monsoon systems during the summer monsoon season. *Atmos. Chem. and*

431 Phys., 15, doi:10.5194/acp-15-11477-2015, 11477-11499, 2015.

432 Fadnavis, S., Semeniuk, K., Schultz, M. G., Mahajan, A., Pozzoli, L., Sonbawane, S., and Kiefer, M.:
433 Transport pathways of peroxyacetyl nitrate in the upper troposphere and lower stratosphere
434 from different monsoon systems during the summer monsoon season, *Atmos. Chem. Phys.*
435 *Discuss.*, 14, 20159–20195, doi:10.5194/acpd-14-20159-2014, 2014.

436 Fiore, A. M., Horowitz, L. W., Purves, D. W., Levy II, H., Evans, M. J., Wang, Y., Li, Q., and
437 Yantosca, R. M.: Evaluating the contribution of changes in isoprene emissions to surface ozone
438 trends over the eastern United States, *J. Geophys. Res.*, 110, D12303,
439 doi:10.1029/2004JD005485, 2005.

440 Flohn, H.: Large-scale aspects of the summer monsoon in South and East Asia, *J. Meteor. Soc. Japan*,
441 75, 180–186, doi: 551.553.21:551.589.5, 1957.

442 Flohn, H.: Recent investigations on the mechanism of the “Summer Monsoon” of Southern and
443 Eastern Asia, *Proc. Symp. Monsoon of the World*, 1960.

444 Forster, F., Piers, M., and Keith, P. Shine: Radiative forcing and temperature trends from stratospheric
445 ozone changes, *J. Geophys Res*, 102, 10841-10855, 1997.

446 Froidevaux, L., Livesey, N. J., Read, W. G., Jiang, Y. B., Jimenez, C. J., Filipiak, M. J., Schwartz, M.
447 J., Santee, M. L., Pumphrey, H. C., Jiang, J. H., Wu, D. L., Manney, G. L., Drouin, B. J.,
448 Waters, J. W., Fetzer, E. J., Bernath, P. F., Boone, C. D., Walker, K. A., Jucks, K. W., Toon, G.
449 C., Margitan, J. J., Sen, B., Webster, C. R., Christensen, L. E., Elkins, J. W., Atlas, E., Ueb, R.
450 A., and Hendershot, R.: Early validation analyses of atmospheric profiles from EOS MLS on
451 the Aura satellite. *IEEE Trans. Geosci. Remote Sensing* 44, 1106 – 1121, doi:
452 10.1109/TGRS.2006.864366, 2006.

453 Fu, R., Hu, Y. L., Wright, J. S., Jiang, J. H., Dickinson, R.E., Chen, M. X., Filipiak, M., Read, W. G.,
454 Waters, J. W., and Wu, D. L.: Short circuit of water vapor and polluted air to the global
455 stratosphere by convective transport over the Tibetan Plateau, *P. Natl. Acad. Sci. USA*, 103,
456 5664–5669, doi:10.1073/pnas.0601584103, 2006.

457 Ganzeveld, L. and Lelieveld, J.: Dry deposition parameterization in a chemistry general circulation
458 model and its influence on the distribution of reactive trace gases, *J. Geophys. Res.*, 100,
459 20999–21012, doi:10.1029/95JD02266, 1995.

460 Garny, H. and Randel, W. J.: Dynamic variability of the Asian monsoon anticyclone observed in
461 potential vorticity and correlations with tracer distributions, *J. Geophys. Res. Atmos.*, 118,
462 13,421–13,433, doi:10.1002/2013JD020908, 2013.

463 Gettelman, A., Kinnison, D. E., Dunkerton, T. J., and Brasseur, G. P.: Impact of monsoon circulations
464 on the upper troposphere and lower stratosphere, *J. Geophys. Res.*, 109, D22101,
465 doi:10.1029/2004jd004878, 2004.

466 Ghude, S. D., Kulkarni, S. H., Jena, C., Pfister, G. G., Beig, G., Fadnavis, S., and van der A R. J.:
467 Application of satellite observations for identifying regions of dominant sources of nitrogen
468 oxides over the Indian Subcontinent, *J. Geophys. Res.*, 118, 1–15, doi:10.1029/2012JD017811,
469 2013.

470 Goswami, B. N., Krishnamurthy, V., and Annamalai, H.: A broad-scale circulation index for the
471 interannual variability of the Indian summer monsoon. *Q. J. R. Meteorol. soc.*, 125, 611-633,
472 doi: 10.1002/qj.49712555412, 1999.

473 Gu, D., Wang, Y., Smeltzer, C., and Boersma, K. F.: Anthropogenic emissions of NO_x over China:
474 Reconciling the difference of inverse modeling results using GOME-2 and OMI
475 measurements, *J. Geophys. Res. Atmos.*, 119, doi:10.1002/ 2014JD021644, 2014.

476 Hilboll, A., Richter, A., and Burrows, J. P.: Long-term changes of tropospheric NO₂ over megacities
477 derived from multiple satellite instruments, *Atmos. Chem. Phys.*, 13, 4145–4169,
478 doi:10.5194/acp-13-4145-2013, 2013.

482

483 Horowitz, L. W., Walters, S., Mauzerall, D. L., Emmons, L. K., Rasch, P. J., Granier, C., Tie, X.,
484 Lamarque, J., Schultz, M. G., Tyndall, G. S., Orlando, J. J., and Brasseur, G. P.: A global
485 simulation of tropospheric ozone and related tracers, Description and evaluation of MOZART,
486 version 2, *J. Geophys. Res.*, 108, 4784, doi:10.1029/2002JD002853, 2003.

487 Jacob, D. J., Logan, J. A., and Murti, P. P.: Effect of rising Asian emissions on surface ozone in the
488 United States, *Geophys. Res. Lett.*, 26, 2175–2178, doi:10.1029/1999GL900450, 1999.

489 Kärcher B. and U. Lohmann, A parameterization of cirrus cloud formation: Homogeneous freezing of
490 supercooled aerosols, *J. Geophys. Res.* 107, NO. D2, 4010, 10.1029/2001JD000470, 2002.

491 Konopka, P., Groß, J.U., Günther, G., Ploeger, F., Pommrich, R., Müller, R. and Livesey, N.: Annual
492 cycle of ozone at and above the tropical tropopause: observations versus simulations with the
493 Chemical Lagrangian Model of the Stratosphere (CLaMS), *Atmos. Chem. Phys.*, 10(1), 121-
494 132, doi: www.atmos-chem-phys.net/10/121/2010/, 2010.

495 Kunze, M., Braesicke, P., Langematz, U., Stiller, G., Bekki, S., Brühl, C., Chipperfield, M., Dameris,
496 M., Garcia, R. and Giorgetta, M.: Influences of the Indian summer monsoon on water vapor
497 and ozone concentrations in the UTLS as simulated by chemistry-climate models, *J. Clim.*,
498 23(13), 3525-3544, doi: <http://dx.doi.org/10.1175/2010JCLI3280.1>, 2010.

500 Lacis Andrew, A., Donald Wuebbles, J., and Jennifer Logan A., Radiative Forcing of climate by
501 Changes in the Vertical Distribution of Ozone, *J. Geophys. Res.*, 95 , 9971-9981, doi:
502 10.1029/JD095iD07p09971, 1990.

503 Lawrence, M. G.: Atmospheric science: Asia under a high-level brown cloud, *Nat. Geosci.*, 4, 352–
504 353, doi:10.1038/ngeo1166, 2011.

505 Lei, W., Zhang, R., Tie, X., and Hess, P.: Chemical characterization of ozone formation in the
506 Houston-Galveston area. *J. Geophys. Res.*, 109, doi: 10.1029/2003JD004219, 2004.

507 Li, C. and Yanai M.: The onset and interannual variability of the Asian summer monsoon in relation to
508 land–sea thermal contrast, *J. Clim.* 9: 358–375, doi: [http://dx.doi.org/10.1175/1520-0442\(1996\)009<0358:TOAIVO>2.0.CO;2](http://dx.doi.org/10.1175/1520-0442(1996)009<0358:TOAIVO>2.0.CO;2), 1996.

509 Li, Q., Jiang, J. H., Wu, D. L., Read, W. G., Livesey, N. J., Waters, J. W., Zhang, Y., Wang, B.,
510 Filipiak, M. J., Davis, C. P., Turquety, S., Wu, S., Park, R. J., Yantosca, R. M., and Jacob, D. J.:
511 Convective outflow of south Asian pollution: a global CTM simulation compared with EOS
512 MLS observations, *Geophys. Res. Lett.*, 32, doi: <http://dx.doi.org/10.1029/2005GL022762>,
513 doi: 10.1029/2005GL022762, 2005.

514 Livesey, N. J., Read, W. G., Filipiak, M. J., Froidevaux, L., Harwood, R. S., Jiang, J. H., Jimenez, C.,
515 Pickett, H. M., Pumphrey, H. C., Santee, M. L., Schwartz, M. J., Waters, J. W., and Wu, D. L.:
516 EOS MLS Version 1.5 Level 2 data quality and description document, JPL, California, 2005.

517 Livesey, N. J., Read, W. G., Froidevaux, L., Lambert, A., Manney, G. L., Pumphrey, H. C., Santee, M.
518 L., Schwartz, M. J., Wang, S., Cofield, R. E., Cuddy, D. T., Fuller, R. A., Jarnot, R. F., Jiang, J.
519 H., Knosp, B. W., Stek, P. C., Wagner, P. A., and Wu, D. L.: Version 3.3 Level 2 data quality
520 and description document. Tech Rep. JPL D-33509, Jet Propulsion Laboratory, available at:
521 <http://mls.jpl.nasa.gov> (last access: 17 August 2015), 2011.

522 Lohmann, U., J. Feichter, C. C. Chuang, and J. E. Penner, Predicting the number of cloud droplets in
523 the ECHAM GCM, *J. Geophys. Res.*, 104, 9169 – 9198, 1999.

524 Meehl, G. A.: Coupled land-ocean-atmosphere processes and South Asian monsoon variability,
525 *Science*, 266, 263–267, doi: 10.1126/science.266.5183.263, 1994.

526 Myhre, G., et al., Anthropogenic and natural radiative forcing, in *Climate Change 2013: The Physical
527 Science Basis. Contribution of Working Group I to the Fifth Assessment Report of the
528 Intergovernmental Panel on Climate Change*, edited by T. F. Stocker et al., pp. 659–740,
529 Cambridge Univ. Press, Cambridge, U. K., and New York, 2013.

530 Park, M., Randel, W. J., Emmons, L. K., Bernath, P. F., Walker, K. A., and Boone, C. D.: Chemical
535

536 isolation in the Asian monsoon anticyclone observed in Atmospheric Chemistry Experiment
537 (ACE-FTS) data, *Atmos. Chem. Phys.*, 8, 3, 757-764, doi: [www.atmos-chem-](http://www.atmos-chem-phys.net/8/757/2008/)
538 [phys.net/8/757/2008/](http://www.atmos-chem-phys.net/8/757/2008/), 2008.

539 Park, M., Randel, W. J., Emmons, L. K., and Livesey, N. J.: Transport pathways of carbon monoxide in
540 the Asian summer monsoon diagnosed from Model of Ozone and Related Tracers (MOZART),
541 *J. Geophys. Res.*, 114, D08303, doi:10.1029/2008jd010621, 2009.

542 Park, M., Randel, W. J., Gettelman, A., Massie, S. T., and Jiang, J.H.: Transport above the Asian
543 summer monsoon anticyclone inferred from Aura Microwave Limb Sounder tracers, *J.*
544 *Geophys. Res.*, 112, D16309, doi:10.1029/2006jd008294, 2007.

545 Park, M., Randel, W. J., Kinnison, D. E., Garcia, R. R., and Choi, W.: Seasonal variation of methane, water vapour, and
546 nitrogen oxides near the tropopause: Satellite observations and model simulations, *J. Geophys. Res.*, 109,
547 D03302, doi:10.1029/2003JD003706, 2004.

548 Penki, R. K. and Kamra, A. K.: Lightning distribution with respect to the monsoon trough position
549 during the Indian summer monsoon season, *J. Geophys. Res.*, 118, 4780–4787,
550 doi:10.1002/jgrd.50382, 2013.

551 Ploeger, F., Gottschling, C., Griessbach, S., Groß, J.-U., Guenther, G., Konopka, P., Müller, R., Riese,
552 M., Stroh, F., Tao, M., Ungermann, J., Vogel, B., and von Hobe, M.: A potential vorticity-based
553 determination of the transport barrier in the Asian summer monsoon anticyclone, *Atmos.*
554 *Chem. Phys.*, 15, 13145-13159, doi:10.5194/acp-15-13145-2015, 2015.

555 Pozzoli, L., Bey, I., Rast, J. S., Schultz, M. G., Stier, P., and Feichter, J.: Trace gas and aerosol
556 interactions in the fully coupled model of aerosol-chemistry-climate ECHAM5- HAMMOZ: 1.
557 Model description and insights from the spring 2001 TRACE-P experiment, *J. Geophys. Res.*,
558 113, D07308, doi:10.1029/2007JD009007, 2008a.

559 Pozzoli, L., Bey, I., Rast, J. S., Schultz, M. G., Stier, P., and Feichter, J.: Trace gas and aerosol
560 interactions in the fully coupled model of aerosol-chemistry-climate ECHAM5- HAMMOZ: 2.
561 Impact of heterogeneous chemistry on the global aerosol distributions, *J. Geophys. Res.*, 113,
562 D07309, doi:10.1029/2007JD009008, 2008b.

563 Pozzoli, L., Janssens-Maenhout, G., Diehl, T., Bey, I., Schultz, M. G., Feichter, J., Vignati, E., and
564 Dentener, F.: Re-analysis of tropospheric sulfate aerosol and ozone for the period 1980–2005
565 using the aerosol-chemistry-climate model ECHAM5-HAMMOZ, *Atmos. Chem. Phys.*, 11,
566 9563–9594, doi:10.5194/acp-11-9563-2011, 2011.

567 Rajeevan M., Bhate J., Kale J.D and Lal B.: Development of High Resolution Daily Gridded Rainfall
568 Data for the Indian Region, *Met. Monograph Climatology No. 22/2005*, National Climate
569 Centre India Meteorological Department. Pune 411 005, India, 2005.

570 Rajagopalan, B., and Molnar, P.: Signatures of Tibetan Plateau heating on Indian summer monsoon
571 rainfall variability, *J. Geophys. Res. Atmos.*, 118, 1170–1178, doi:10.1002/jgrd.50124, 2013.

572 Ranalkar, M. R. and Chaudhari, H. S.: Seasonal variation of lightning activity over the Indian
573 subcontinent, *Meteorol. Atmos. Phys.*, 104, 125–134, doi: 10.1007/s00703-009-0026-7, 2009.

574 Randel, W. J., and Park M.: Deep convective influence on the Asian summer monsoon anticyclone and
575 associated tracer variability observed with Atmospheric Infrared Sounder (AIRS), *J. Geophys.*
576 *Res.*, 111, D12314, doi:10.1029/2005JD006490, 2006.

577 Randel, W. J., Park, M., Emmons, L., Kinnison, D., Bernath, P., Kaley Walker, A., Boone, C., and
578 Pumphrey, H.: Asian Monsoon Transport of Pollution to the Stratosphere *Science*, 328(5978),
579 611-613, doi: 10.1126/science.1182274, 2010.

580 Randel, W. J., Wu, F., Gettelman, A., Russell, J. M., Jawodny, J. M., and Oltmans, S. J.: Seasonal
581 variation of water vapor in the lower stratosphere observed in Halogen Occultation Experiment
582 data, *J. Geo-phys. Res.*, 106, 14,313 – 14,325, doi: 0148-0227/01/2001JD900048509.00, 2001.

583 Rap, A., Richards, N., A., D., Forster, P., M., Monks, S., Arnold, S., R., Chipperfield, M.: Satellite

584 constraint on the tropospheric ozone radiative effect, *Geophys. Res. Lett.*, 42, [5074-5081](https://doi.org/10.1002/2015GL064037).doi:10.1002/2015GL064037, 2015.

585

586 Revell, L. E., Tummon, F., Stenke, A., Sukhodolov, T., Coulon, A., Rozanov, E., Garny, H., Grewe, V.,
587 and Peter, T.: Drivers of the tropospheric ozone budget throughout the 21st century under the
588 medium-high climate scenario RCP 6.0, *Atmos. Chem. Phys.*, 15, 5887-5902, doi:10.5194/acp-
589 15-5887-2015, 2015.

590 Richter, A., John Burrows, P., Hendrik, N., Granier C., and Niemeier, U.: Increase in tropospheric
591 nitrogen dioxide over China observed from space; 437, doi:10.1038/nature04092, 2005.

592 Riese, M., Ploeger, F., Rap, A., Vogel, B., Konopka, P., Dameris, M. and Forster, P.: Impact of
593 uncertainties in atmospheric mixing on simulated UTLS composition and related radiative
594 effects, *J. Geophys. Res.: Atmos.*, 117(D16), doi: 10.1029/2012JD017751, 2012.

595 Rodwell, M. J. and Hoskins, B. J.: Monsoons and the dynamics of deserts, *QJRMS*, 122(534), 1385-
596 1404, doi: 10.1002/qj.49712253408, 1995.

597 Roeckner, E., Bauml, G., Bonaventura, L., Brokopf, R., Esch, M., Giorgetta, M., Hagemann, S.,
598 Kirchner, I., Kornblueh, L., Manzini, E., Rhodin, A., Schlese, U., Schulzweida, U., and
599 Tompkins, A.: The atmospheric general circulation model ECHAM5: Part 1, Tech. Rep. 349,
600 Max Planck Institute for Meteorology, Hamburg, 2003.

601 Sander, S. P., Fried, R. R., Barker, J. R., Golden, D. M., Kurylo, M. J., Wine, P. H., J. Abbatt, P. D., 25
602 Burkholder, J. B., Kolb, C. E., Moortgat, G. K., Huie, R. E., and Orkin, V. L.: Chemical
603 kinetics and photochemical data for use in atmospheric studies, evaluation number 14, JPL
604 Publ. 02-25, Jet Propul. Lab., Calif. Inst. Of Technol., Pasadena, available at:
605 http://jpldataeval.jpl.nasa.gov/pdf/JPL_02-25_rev02.pdf, 2003.

606 Schneider, P. and van der A. R. J.: A global single-sensor analysis of 2002–2011 tropospheric nitrogen
607 dioxide trends observed from space, *J. Geophys. Res.*, 117, D16309,
608 doi:10.1029/2012JD017571, 2012.

609 Schoeberl, M. R., Duncan, B. N., Douglass, A. R., Waters, J., Livesey, N., Read, W., and Filipiak, M.:
610 The carbon monoxide tape recorder. *Geophys. Res. Lett.*, 33(12), doi:
611 10.1029/2006GL026178, 2006.

612 Schultz, M. G., Heil, A., Hoelzemann, J. J., Spessa, A., Thonicke, K., Goldammer, J. G., Held, A. C.,
613 Pereira, J. M. C., and van het Bolscher, M.: Global wildland fire emissions from 1960 to 2000,
614 *Global Biogeochem. Cy.*, 22, GB2002, doi:10.1029/2007GB003031, 2008.

615 Schultz, M., Backman, L., Balkanski, Y., Bjoerndalsaeter, S., Brand, R., Burrows, J., Dalsoeren, S., de
616 Vasconcelos, M., Grodtmann, B., Hauglustaine, D., Heil, A., Hoelzemann, J., Isaksen, I.,
617 Kaurola, J., Knorr, W., Ladstaetter-Weienmayer, A., Mota, B., Oom, D., Pacyna, J., Panasiuk,
618 D., Pereira, J., Pulles, T., Pyle, J., Rast, S., Richter, A., Savage, N., Schnadt, C., Schulz, M.,
619 Spessa, A., Staehelin, J., Sundet, J., Szopa, S., Thonicke, K., van het Bolscher, M., van Noije,
620 T., van Velthoven, P., Vik, A. and Wittrock, F.: REanalysis of the TROospheric chemical
621 composition over the past 40 years (RETRO). A long-term global modeling study of
622 tropospheric chemistry. Final Report, Tech. rep., Max Planck Institute for Meteorology,
623 Hamburg, Germany, 2007.

624 Schultz, M.G., Heil A., Hoelzemann, J. J., Spessa, A., Thonicke, K., Goldammer, J., Held, A.C,
625 Pereira, J. M., Van Het Bolscher, M.: Global Wildland Fire Emissions from 1960 to 2000,
626 doi:10.1029/2007GB003031 , *Global Biogeochemical Cycles* 22 (GB2002) : 17 PP, 2005

627 Sillman, S.: The use of NO_y, H₂O₂, and HNO₃ as indicators for ozone-NO_x-hydrocarbon sensitivity in
628 urban locations. *J. Geophys. Res.*, 100, 14,175–14,188, doi: 10.1029/94JD02953, 1995.

629 Sinha, V., Kumar, V., and Sarkar, C.: Chemical composition of pre-monsoon air in the Indo-Gangetic
630 Plain measured using a new air quality facility and PTR-MS: high surface ozone and strong
631 influence of biomass burning, *Atmos. Chem. Phys.*, 14, 5921–5941, 2014. doi:10.5194/acp-14-

632 5921-2014, 2014.

633 Søvde, O. A., Hoyle, C. R., Myhre, G., and Isaksen, I. S. A.: The HNO₃ forming branch of the HO₂ +
634 NO reaction: pre-industrial-to-present trends in atmospheric species and radiative forcings,
635 *Atmos. Chem. Phys.*, 11, 8929–8943, 2011; doi:10.5194/acp-11-8929-2011, 2011.

636 Stevenson, D. S., P. J. Young, Vaishali, N., Lamarque, J. F., Drew, T., Shindell, Voulgarakis, A., and
637 Skeie R. B.: Tropospheric ozone changes, radiative forcing and attribution to emissions in the
638 Atmospheric Chemistry and Climate Model Intercomparison Project (ACCMIP), *Atmos.*
639 *Chem. Phys.*, 13, 3063-3085, doi:10.5194/acp-13-3063-2013, 2013.

640 Stier, P., Feichter, J., Kinne, S., Kloster, S., Vignati, E., Wilson, J., Ganzeveld, L., Tegen, I., Werner,
641 M., Balkanski, Y., Schulz, M., Boucher, O., Minikin, A., and Petzold, A.: The aerosol-climate
642 model ECHAM5-HAM, *Atmos. Chem. Phys.*, 5, 1125–1156, doi:10.5194/acp-5-1125-2005,
643 2005.

644 Thuburn, J. and Craig, G.C.: On the temperature structure of the tropical stratosphere, *Journal of*
645 *Geophysical Research: Atmospheres*, 107(D2), doi: 10.1029/2001JD000448, 2002.

646 Tie, X. X., Zhang, R., Brasseur, G., Emmons, L., and Lei, W.: Effects of lightning on reactive nitrogen
647 and nitrogen reservoir species in the troposphere, *J. Geophys. Res.-Atmos.*, 106, 3167– 3178,
648 doi:10.1029/2000JD900565, 2001.

649 Tie, X., Madronich, S., Li, G.H., Ying, Z.M., Zhang, R., Garcia, A., Lee-Taylor, and J., Y. Liu.
650 Characterizations of chemical oxidants in Mexico City: a regional chemical/dynamical model
651 (WRF-Chem) study, *Atmos. Environ.*, 41, 1989–2008, doi:10.1016/j.atmosenv.2006.10.053,
652 2007.

653 Tiedtke, M.: A comprehensive mass flux scheme for cumulus parameterization in large-scale models,
654 *Mon. Weather Rev.*, 117(8), 1779–1800, 1989.

655 Tobo, Y., Iwasaka, Y., Zhang, D., Shi, G., Kim, Y. S., Tamura, K., and Ohashi, T.: Summertime
656 “ozone valley” over the Tibetan Plateau derived from ozonesondes and EP/TOMS data,
657 *Geophys. Res. Lett.*, 35, L16801, doi:10.1029/2008GL03434, 2008.

658 Vernier, J.-P., T. D. Fairlie, M. Natarajan, F. G. Wienhold, J. Bian, B. G. Martinsson, S. Crumeyrolle,
659 L. W. Thomason, and Bedka, K.: Increase in upper tropospheric and lower stratospheric
660 aerosol levels and its potential connection with Asian Pollution, *J. Geophys. Res. Atmos.*, 120,
661 1608–1619, doi:10.1002/2014JD022372, 2015.

662 Vinoj, V., Rasch, P.J., Wang, H., Yoon, J.H., Ma, P.L., Landu, K. and Singh, B.: Short-term modulation
663 of Indian summer monsoon rainfall by West Asian dust, *Nature Geoscience*, 7(4), 308-313,
664 doi:10.1038/ngeo2107, 2014.

665 Vogel, B., Günther, G., Müller, R., Grooß, J.-U., and Riese, M.: Impact of different Asian source
666 regions on the composition of the Asian monsoon anticyclone and of the extratropical
667 lowermost stratosphere, *Atmos. Chem. Phys.*, 15, 13699-13716, doi:10.5194/acp-15-13699-
668 2015, 2015.

669 Vogel, B., Günther, G., Müller, R., Grooß, J.-U., Afchine, A., Bozem, H., Hoor, P., Krämer, M., Müller,
670 S., Riese, M., Rolf, C., Spelten, N., Stiller, G. P., Ungermann, J., and Zahn, A.: Long-range
671 transport pathways of tropospheric source gases originating in Asia into the northern lower
672 stratosphere during the Asian monsoon season 2012, *Atmos. Chem. Phys.*, 16, 15301-15325,
673 doi:10.5194/acp-16-15301-2016, 2016.

674 Waters, J. W., Froidevaux, L., Harwood, R.S., Jarnot, R.F., Pickett, H. M., Read, W. G., Siegel, P. H.,
675 Cofield, R. E., Filipiak, M. J., Flower, D. A., Holden, J. R., Lau, G. K., Livesey, N. J., Manney,
676 G. L., Pumphrey, H. C., Santee, M. L., Wu, D. L., Cuddy, D. T., Lay, R. R., Loo, M. S., Perun,
677 V. S., Schwartz, M. J., Stek, P. C., Thurstans, R. P., Boyles, M. A., Chandra, S., Chavez, M. C.,
678 Chen, G. S., Chudasama, B. V., Dodge, R., Fuller, R. A., Girard, M.A., Jiang, J. H., Jiang, Y.,
679 Knosp, B. W., LaBelle, R. C., Lee, K. A., Miller, D., Oswald, J. E., Patel, N. C., Pukala, D.

681 M., Quintero, O., Scaff, D. M., Snyder, W. V., Tope, M. C., Wagner, P. A., and Walch, M. J.:
682 The Earth Observing System Microwave LimbSounder (EOS MLS) on the Aura satellite.
683 IEEE Trans, Geosci., Remote Sensing, 44, 1075 – 1092, doi: 10.1109/TGRS.2006.873771,
684 2006.

685 Wild, O., and Akimoto, H.: Intercontinental transport of ozone and its precursors in a three-
686 dimensional global CTM, *J. Geophys. Res.*, 106(D21), 27729-27744, doi:
687 <http://dx.doi.org/10.1029/2000JD000123>, 2001.

688 Wu, G. X., and Zhang, Y. S.: Tibetan Plateau forcing and the timing of the monsoon onset over South
689 Asia and the South China Sea, *Mon Wea Rev* 126:913–927, doi:
690 [http://dx.doi.org/10.1175/1520-0493\(1998\)126<0913:TPFATT>2.0.CO;2](http://dx.doi.org/10.1175/1520-0493(1998)126<0913:TPFATT>2.0.CO;2), 1998.

691 Xiong, X., Houweling S., Wei J., Maddy E., Sun F., and Barnet C.: Methane plume over south Asia
692 during the monsoon season: satellite observation and model simulation, *Atmos. Chem. Phys.*,
693 9, 783–794, doi:10.5194/acp-9-783-2009, 2009.

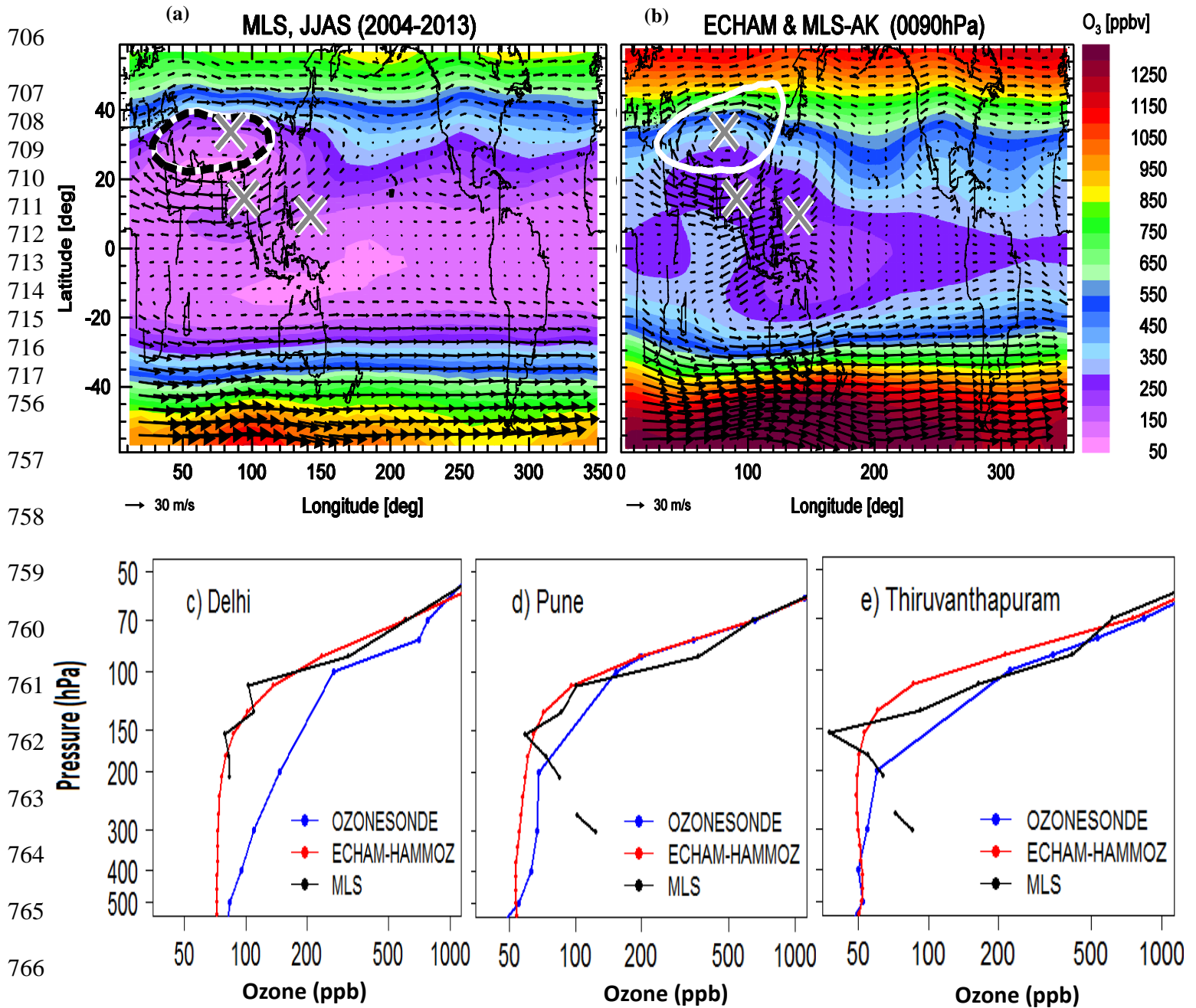
694 Yamaji, K., T. Ohara, I. Uno, H. Tanimoto, J. Kurokawa, and Akimoto H.: Analysis of the seasonal
695 variation of ozone in the boundary layer in East Asia using the Community Multiscale Air
696 Quality model: what controls surface ozone levels over Japan?, *Atmos. Environ.*, 40, 1856–
697 1868, 2006.

698 Yanai, M., Li, C., Song, Z.: Seasonal heating of the Tibetan Plateau and its effects on the evolution of
699 the Asian summer monsoon, *J Meteor Soc Japan*, 70, 189–221, 1992.

700 Zhang, R.W., Lei, X., and Hess, T. P.: Industrial emissions cause extreme diurnal urban ozone
701 variability. *Proc. Natl. Acad. Sci.*, 101, 6346–6350, doi: 10.1073/pnas.0401484101, 2004.

702 Zhao, B., Wang, S. X., Liu, H., Xu, J. Y., Fu, K., Klimont, Z., Hao, J. M., He, K. B., Cofala, J., and
703 Amann, M.: NO_x emissions in China: historical trends and future perspectives, *Atmos. Chem.*
704 *Phys.*, 13, 9869–9897, doi:10.5194/acp-13-9869-2013, 2013.

705



768 Figure 1: Distribution of ozone mixing ratio (ppb) during the monsoon season (June-September)
 769 obtained from (a) MLS observations at 100 hPa, and (b) from ECHAM-HAMMOZ at 90hPa. Black
 770 arrows indicate wind vectors, the black dashed contour shows the PV-gradient based transport barrier
 771 of the anticyclone (calculated following Ploeger et al., 2015), and the white contour shows the 270m
 772 geopotential height anomaly, corresponding to the anticyclone edge definition by Barret et al. (2016)
 773 Meteorological data shows climatological July fields from ERA-Interim reanalysis (a) ERA-Interim

774 reanalysis and (b) ECHAM5-HAMMOZ. The ECHAM5-HAMMOZ ozone distribution is smoothed
775 using the MLS averaging kernel. Grey crosses highlight the regions of the Tibetan plateau, Bay of
776 Bengal and South China Sea. Bottom panels show the vertical distribution of seasonal (June-
777 September) mean ozone mixing ratios (ppb) from ozonesonde (2001-2009), MLS (2004-2013) and
778 ECHAM5-HAMMOZ CTRL simulation at the (c) Delhi, (d) Pune, and (e) Thiruvananthpuram Indian
779 stations.
780

781

782

783

784

785

786

787

788

789

790

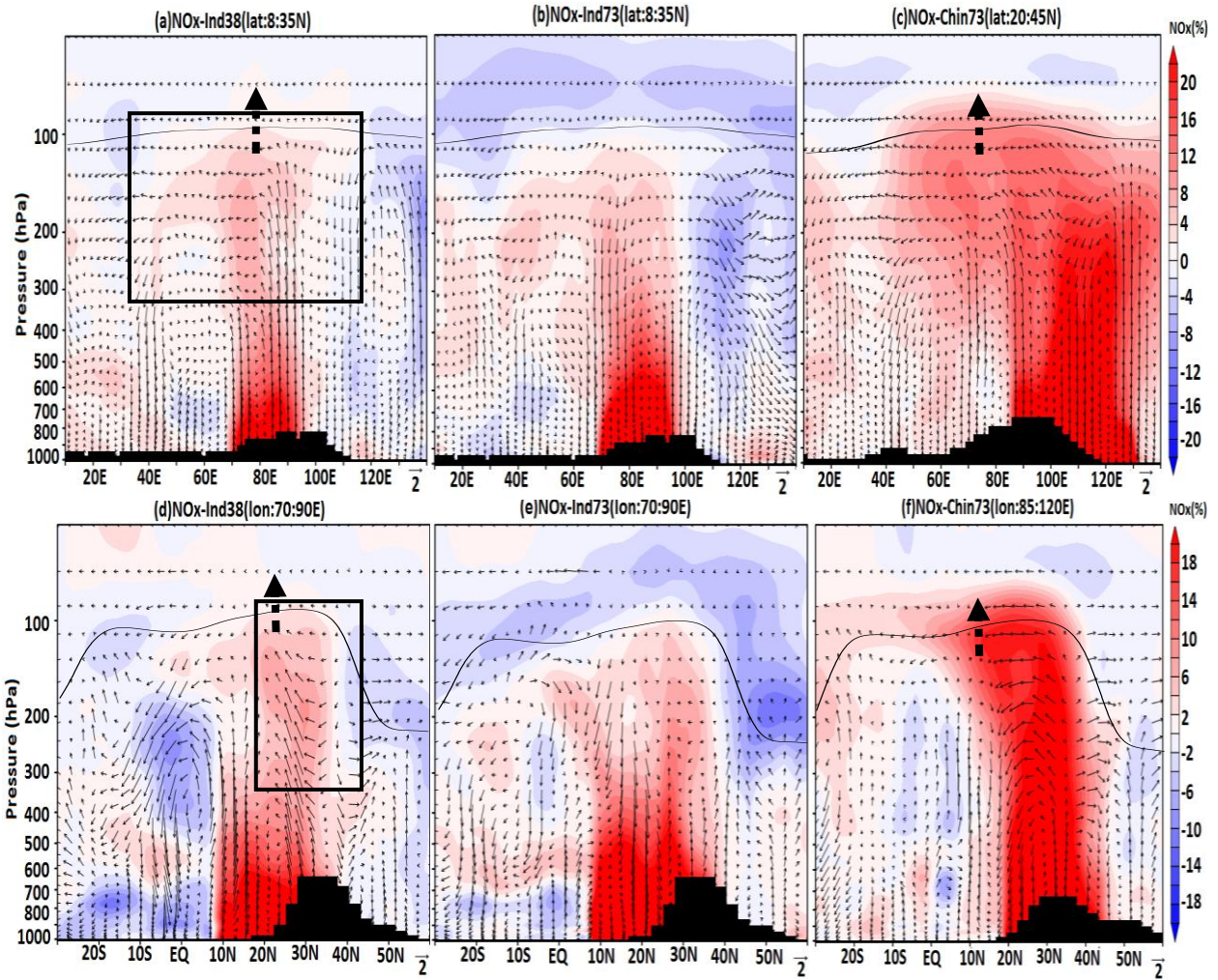
791

792

793

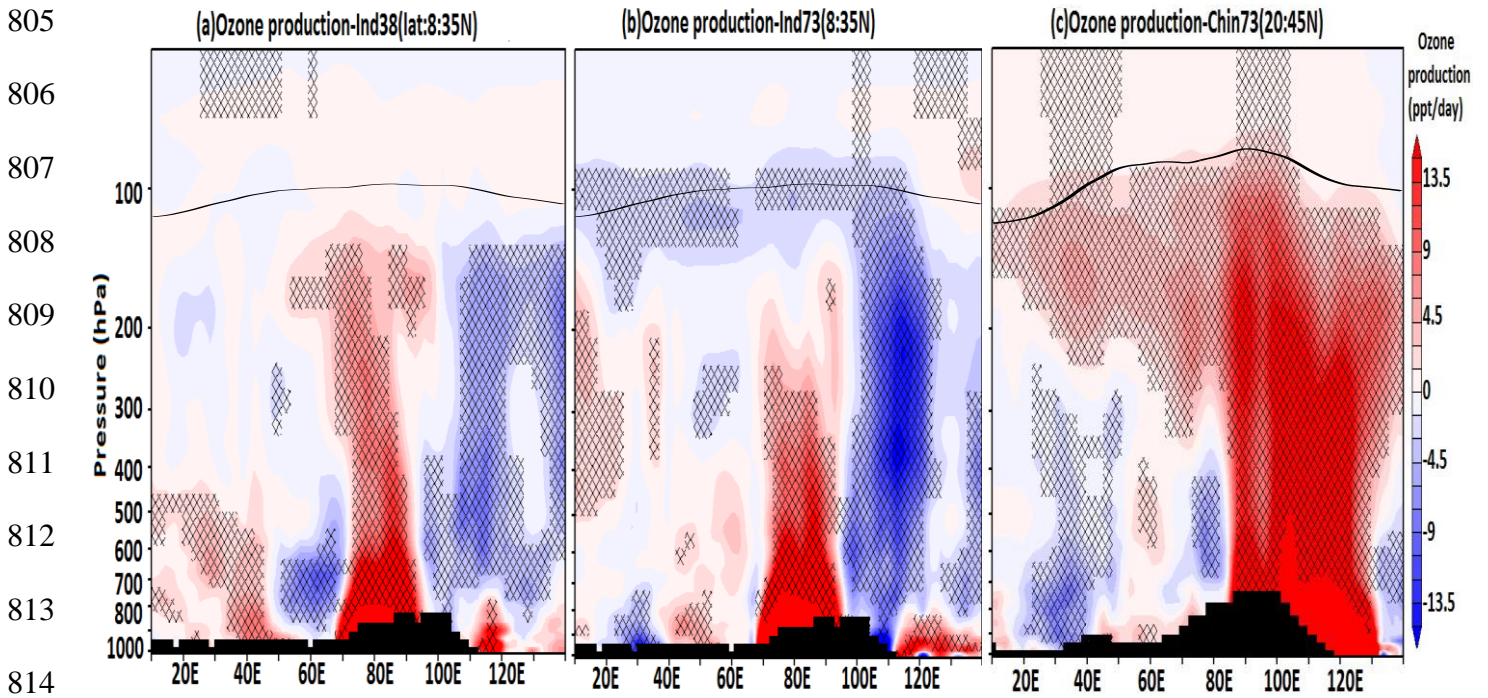
794

795



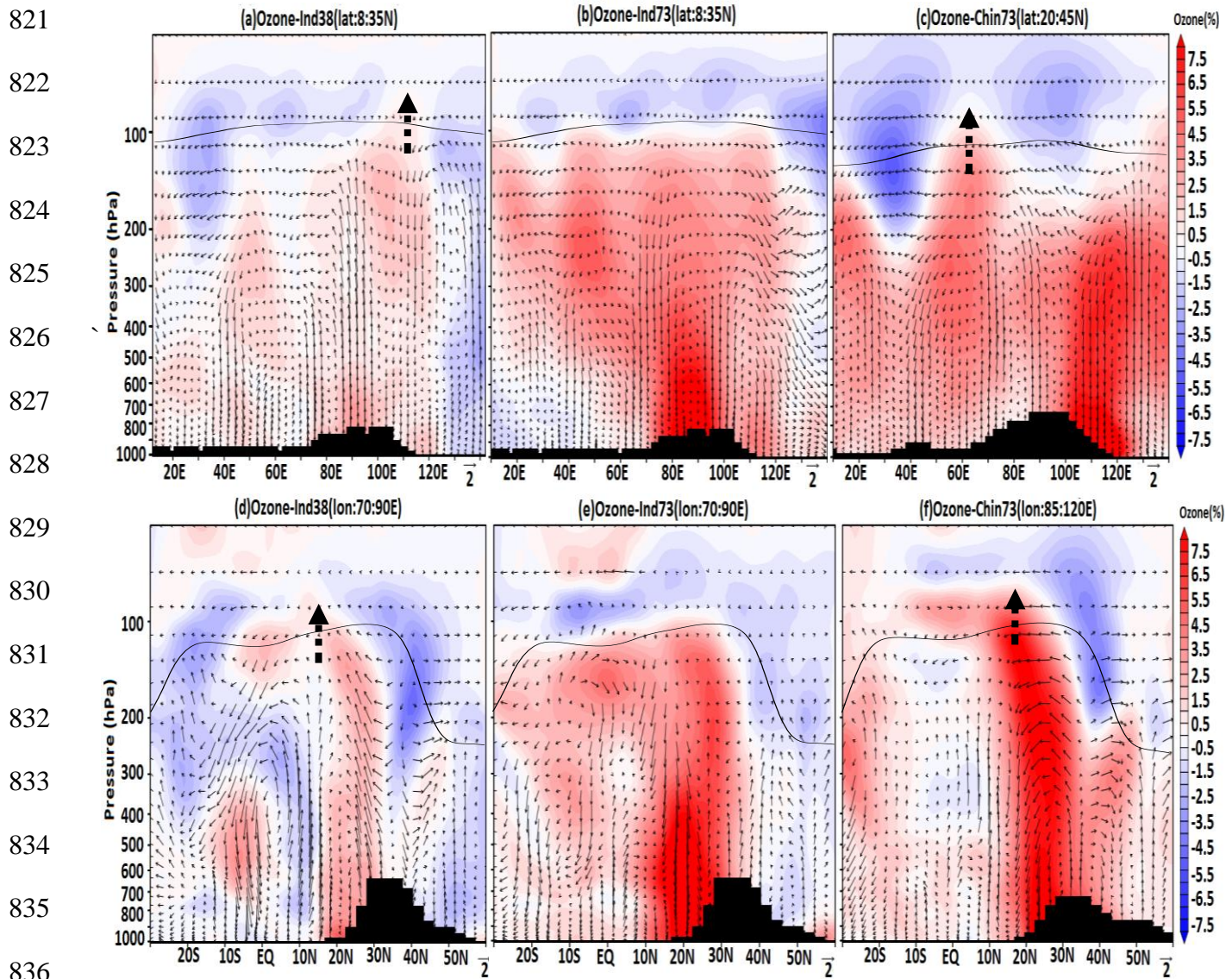
796 Figure 2: Longitude pressure cross-sections of percentage NO_x anomalies averaged for the monsoon
797 season (June-September) obtained from (a) Ind38 (averaged over 8°N - 35°N), (b) Ind73 (averaged over
798 8°N - 35°N), and (c) Chin73 (averaged over 20°N - 45°N) simulations. Latitude pressure cross-sections of
799 percentage NO_x anomalies averaged for the monsoon season (June-September) obtained from (d)
800 Ind38 (averaged over 70°E - 90°E), (e) Ind73 (averaged over 70°E - 90°E), and (f) Chin73 (averaged over
801 85°E - 120°E) simulations. Black arrows indicate wind vectors (the vertical velocity field has been
802 scaled by 300), the black line represents the tropopause, and the black dashed arrows indicate the cross
803 tropopause transport. The black boxes show the outline of the anticyclone.

804

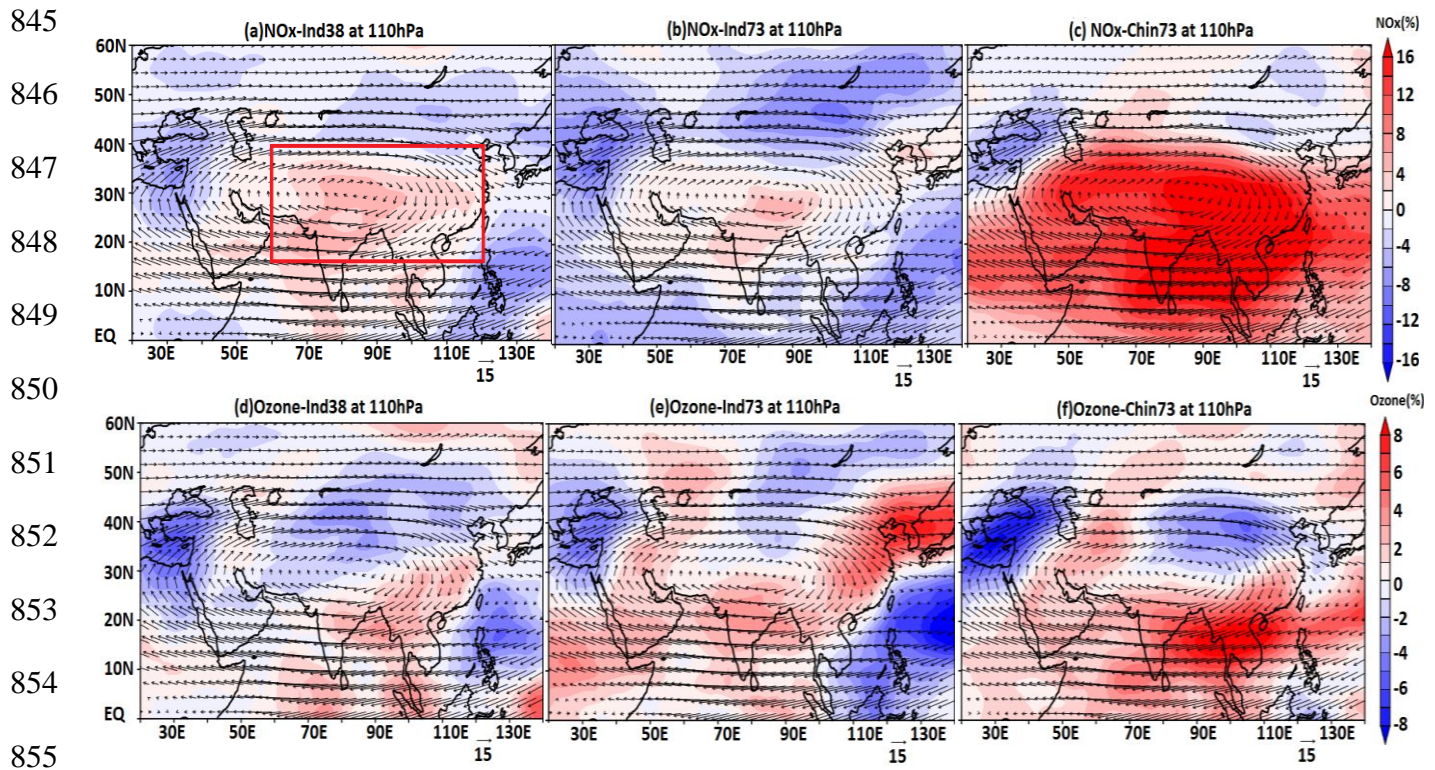


815

816 Figure 3: Longitude pressure cross-section of changes in net ozone production (ppt/day) due to
 817 enhanced NO_x with respect to the CTRL simulation, averaged for the monsoon season (June-
 818 September) obtained from (a) Ind38 (averaged over 8°N-35°N), (b) Ind73 (averaged over 8°N-35°N),
 819 and (c) Chin73 (over 20°N-45°N) simulations. The black line shows the tropopause while black hatched
 820 lines indicate 95% confidence level.



837 Figure 4: Longitude pressure cross-section of percentage ozone anomalies averaged for the monsoon
 838 season (June-September) obtained from (a) Ind38 (averaged over 8°N-35°N), (b) Ind73 (averaged over
 839 8°N-35°N), and (c) Chin73 (averaged over 20°N-45°N) simulations. Latitude pressure cross-section of
 840 percentage ozone anomalies averaged for the monsoon season (June-September) obtained from (d)
 841 Ind38 (averaged over 70°E-90°E), (e) Ind73 (averaged over 70°E-90°E), and (f) Chin73 (averaged over
 842 85°E-120°E) simulations. Black arrows indicate wind vectors. The vertical velocity field has been
 843 scaled by 300. The black line represents the tropopause, and the black dashed arrows indicate the cross
 844 tropopause transport.



856 Figure 5: Latitude-longitude cross-section of percentage NO_x anomalies averaged for the monsoon
857 season (June-September) at 110 hPa obtained from (a) Ind38, (b) Ind73, and (c) Chin73 simulations.
858 Panels (d-f) show the same but for percentage ozone anomalies at 110 hPa for the (d) Ind38, (e) Ind73,
859 and (f) Chin73 simulations. Black arrows indicate horizontal winds at 110 hPa. The red box in panel (a)
860 indicates the ASM anticyclone region used to compute the associated radiative forcing regional
861 average.

862

863

864

865

866

867

868

869

870

871

872

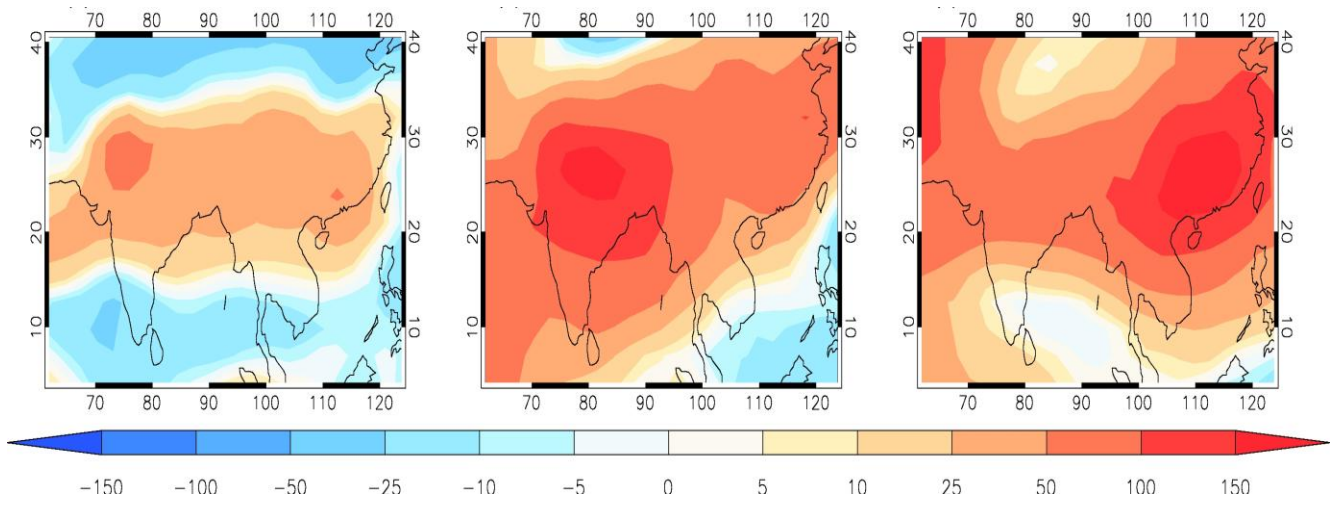


Figure 6: Latitude-longitude distribution of changes in ozone radiative forcing (in mW m^{-2}) for the (a) Ind38, (b) Ind73, and (c) Chin73 perturbed simulations, compared to the CTRL simulation.

873

874

875

876

877

878

879

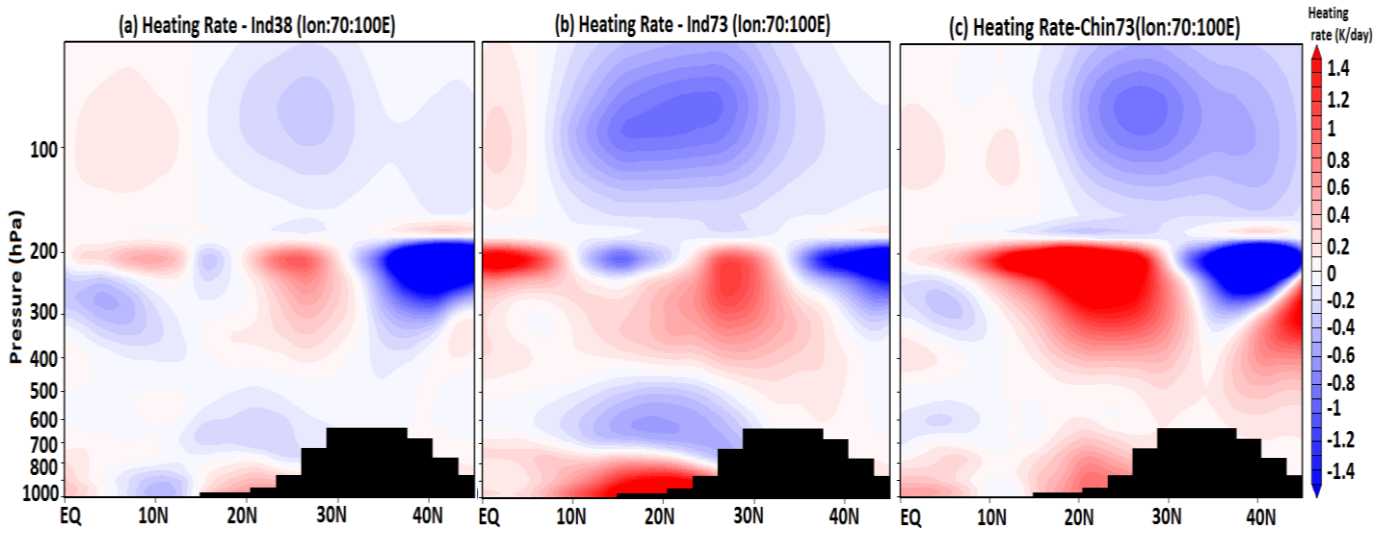
880

881

882

883

884 Figure 7: Latitude- pressure distribution of ozone heating rate changes (in K/day) for the (a) Ind38
885 (averaged over 70°-100°E), (b) Ind73 (averaged 70°-100°E), and (c) Chin73 (averaged over 70° -100°
886 E) perturbed simulations, compared to the CTRL simulation.



887

888

889

890

891

892

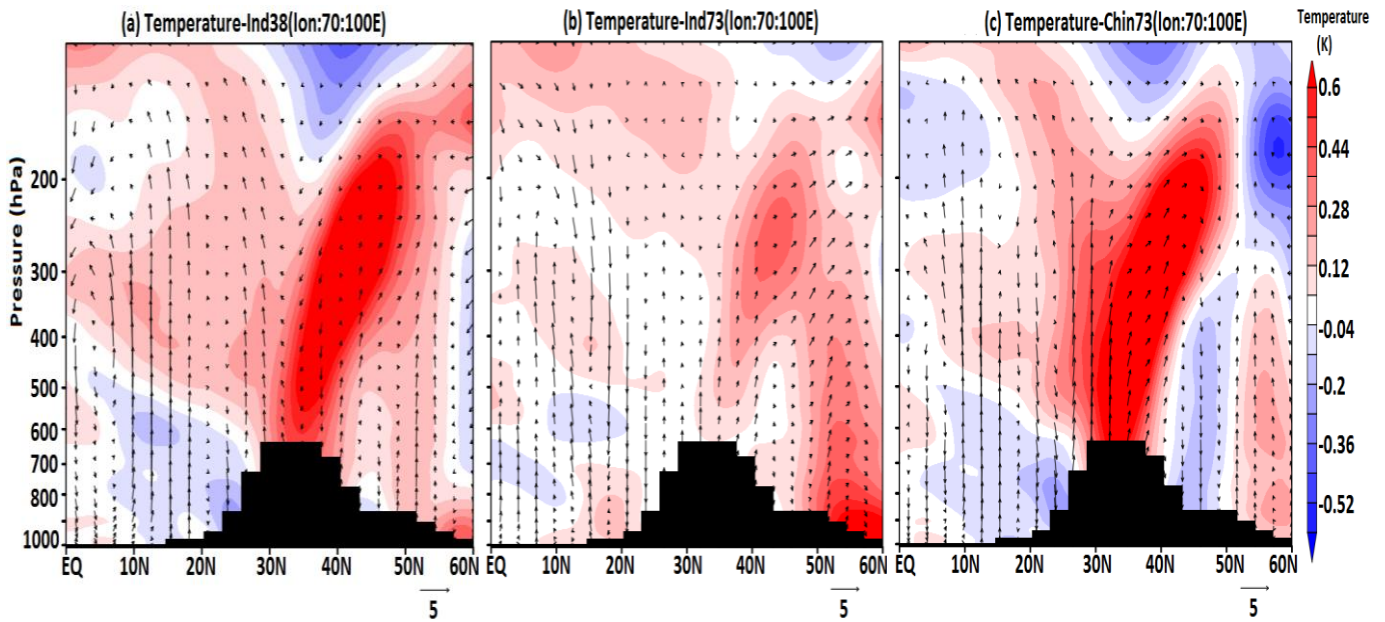
893

894

895

896

897



898 Figure 8: Latitude pressure cross-section of temperature anomalies (K) averaged for the monsoon
899 season (June-September) and over 70°E-100°E obtained from (a) Ind38-CTRL, (b) Ind73-CTRL, and
900 (c) Chin73-CTRL simulations. Black arrows indicate wind vectors (the vertical velocity field has been
901 scaled by 300).

902

903

904

905

906

907

908

909

910

911

912

913

914

915

916

917

918

919

920

921

922

923

924

925

926

927

928

929

930

931

932

933

934

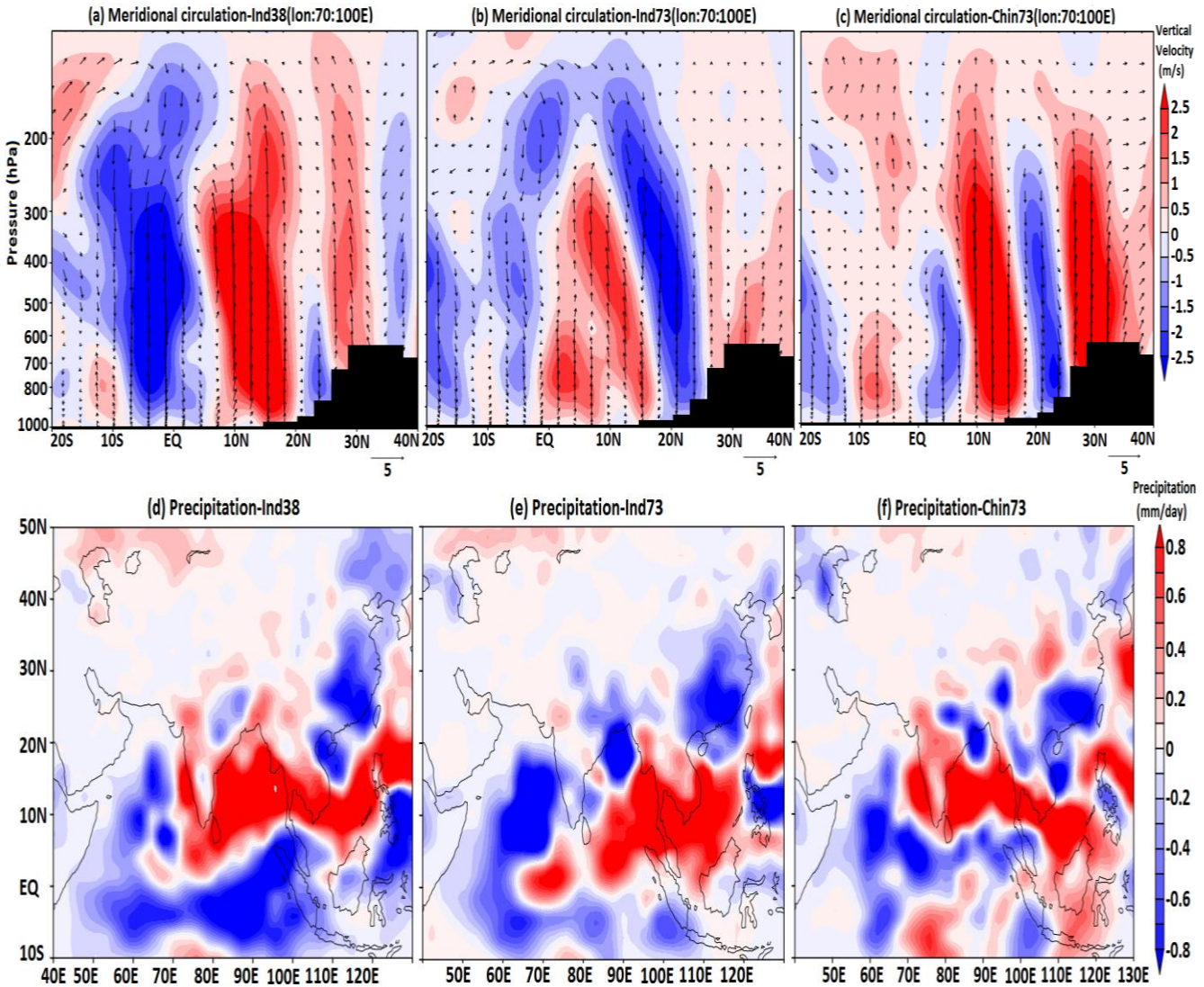


Figure 9: Difference in the meridional circulation due to enhanced NO_x emissions averaged for the monsoon season (June-September) and over 70°E - 100°E for (a) Ind38-CTRL (b) Ind73-CTRL (c) Chin73-CTRL simulations. Shaded contours indicate the anomalies in vertical velocity (m/s). The vertical velocity field has been scaled by 300. Precipitation anomalies (mm/day) averaged for the monsoon season (June-September) obtained from (d) India38-CTRL (e) Ind73-CTRL, and (f) Chin73-CTRL simulations.